On the Accuracy of Zernike Moments for Image Analysis

Simon X. Liao and Miroslaw Pawlak, *Member*, *IEEE*

Abstract—In this paper, we give a detailed analysis of the accuracy of Zernike moments in terms of their discretization errors and the reconstruction power. It is found that there is an inherent limitation in the precision of computing the Zernike moments due to the geometric nature of a circular domain. This is explained by relating the accuracy issue to a celebrated problem in analytic number theory of evaluating the lattice points within a circle.

Index Terms—Zernike moments, geometric error, lattice points, circle problem, image reconstruction.

1 Introduction

One of the fundamental issues in the design of an imagery recognition system is related to the selection of appropriate numerical features in order to achieve high recognition performance. Furthermore, the features to be extracted from an object of interest should be invariant with respect to its position, size, and orientation. Moment descriptors provide characteristics of an object that uniquely represent its shape and, moreover, are invariant to linear transformations. Researchers have been interested in the utilization of moments for object characterization and recognition since the 1960s [4]. We refer to [12] and [17] for an extensive overview of moment-based techniques and applications.

Some nonlinear combinations of standard geometric moments are invariant under image translation, scale change, and rotation only when they are computed from the original analog image. In practice, however, one observes the digitized, and often noisy version of the image and the invariant properties are satisfied only approximately. The error analysis of the resulting inaccuracies in moment computing has been rarely addressed. In [15], the problem of the discretization error for the case of the geometric moments is studied. See also [11] and [9] for further studies in this direction.

Traditionally, geometric moments $\{M_{pq}\}$, being the projection of an image function $f(x, y)$ onto the monomials $\{x^p y^q\}$, have been utilized. The set of functions $\{x^p y^q\}$, however, is not orthogonal implying that $\{M_{pq}\}$ contain redundant information.

Teague [14] has suggested the use of orthogonal moments based on a certain class of orthogonal polynomials to overcome the aforementioned shortcomings associated with the geometric moments. In particular, he has proposed to use the orthogonal moments defined in terms of the Legendre and Zernike polynomials. A number of studies on the Legendre and Zernike moments reconstruction and classification power has been carried out [1], [7], [8], [9], [11], [12], [14], [16], [17]. Nevertheless, the error analysis and analytic characterization of the orthogonal moments have been rarely investigated. In [11] and [9], the vulnerability of the orthogonal Legendre moments against discretization and noise has been examined. The Legendre moments, however, despite their good reconstruction properties, are not invariant to linear operations. The method of Zernike orthogonal moments, which are invariant to linear transformations, has been used as an attractive alternative. Some experimental studies and applications in image analysis with the Zernike moments have been performed and implemented [1], [7], [16], [17]. Fast algorithms for calculating the Zernike moments are proposed in [10]. Applications in optical engineering are discussed in [14].

In this paper, the detailed discretization error analysis for the Zernike moments is carried out. Our main result, concerned with so-called geometric error, reveals an inherent limitation in the accuracy of the Zernike moments computing related to the fact that the Zernike moments are confined to a unit circle rather than a square. This is explained by using a celebrated problem in the analytic number theory referred to as the lattice points of a circle, due originally to Gauss and further studied by a number of authors. See [6] and Section 3.1 in this paper for an historical account of this problem.

The numerical accuracy of the Zernike moments computing is also examined. Some new techniques utilizing various two-dimensional numerical integration methods for increasing the overall accuracy of the Zernike moments are proposed. The performance of our algorithms is assessed by means of the image reconstruction. By reconstructing an image from the extracted moments, one may visually check how many moments are required to capture its essential structure [16], [17]. This is illustrated by reconstructing a set of Chinese characters with Zernike moments.

The paper is organized as follows. Section 2 gives a brief review of the Zernike moments. Section 3 presents the accuracy analysis of the digital approximation of the Zernike moments. The image reconstruction scheme from the computed Zernike moments is studied in Section 4. Experimental studies utilizing a set of Chinese characters are presented in Section 5.

2 Zernike Moments

The use of the Zernike moments in image analysis was pioneered by Teague [14]. Since then, the Zernike moments have been frequently utilized for a number of image processing and computer vision tasks [1], [7], [8], [10], [12], [16], [17].

In order to define the Zernike moments, we need to introduce the concept of Zernike functions. A set of complex orthogonal functions with a simple rotational property which forms a complete orthogonal basis over the class of square integrable functions defined over the unit disk was introduced by Zernike [18]. The (p, q) order Zernike function is defined as

$$V_{pq}(x, y) = R_{pq}(\rho) \exp(jq\theta), \qquad x^2 + y^2 \le 1, \tag{1}$$

where $\rho = \sqrt{x^2 + y^2}$ is the length of the vector from the origin to the pixel (x, y), and $\theta = \arctan(y/x)$ is the angle between the vector and the x axis. In (1), $R_{pq}(\rho)$ is a polynomial in ρ of degree $p \ge 0$, containing no power of ρ lower than $|q|$. See, e.g., [16] for an explicit formula of $R_{pq}(\rho)$. The integer q takes positive, negative, or zero values, and it satisfies

$$|q| \le p, \tag{2}$$

where $p - |q|$ is an even number.

It has been shown in [2] that any polynomial of degree p will be invariant with respect to rotations of axes about the origin if and only if the polynomial is of the form given by (1). The Zernike system is a distinguish case of such a class of invariant polynomials which satisfies the condition in (2).

The orthogonality relation for $\{V_{pq}(x, y)\}$ is

$$\iint_D V_{pq}^*(x, y) V_{p'q'}(x, y) dxdy = \frac{\pi}{p+1} \delta_{pp'} \delta_{qq'}, \tag{3}$$

where $\delta_{pp'} = 1$ if $p = p'$ and 0 otherwise.

- *S. Liao is with the Department of Business Computing, the University of Winnipeg, 515 Portage Avenue, Winnipeg, Manitoba, Canada, R3B 2E9. E-mail: Simon.Liao@UWinnipeg.ca.*
- *M. Pawlak is with the Department of Electrical and Computer Engineering, the University of Manitoba, Winnipeg, Manitoba, Canada, R3T 5V6. E-mail: pawlak@ee.umanitoba.ca.*

Manuscript received 13 May 1997; revised 15 Sept. 1998. Recommended for acceptance by R. Chin.
For information on obtaining reprints of this article, please send e-mail to: tpami@computer.org, and reference IEEECS Log Number 107413.

The completeness and orthogonality of $\{V_{pq}(x, y)\}$ allow us to represent any square integrable image function $f(x, y)$ defined on the unit disk in the following series:

$$f(x,y) = \sum_{p=0}^{\infty} \sum_{q=-p}^{p} \tau_p A_{pq} V_{pq}(x,y), \quad p - |q| = \text{even}, \tag{4}$$

where, due to (3), $\tau_p = \frac{p+1}{\pi}$ is the normalizing constant and A_{pq} is the Zernike moment of order p with repetition q, i.e.,

$$A_{pq} = \int\int_D f(x,y) V_{pq}^*(x,y) dxdy. \tag{5}$$

The fundamental feature of the Zernike moments is their rotational invariance. If $f(x, y)$ is rotated by an angle α, then we can obtain that the Zernike moment A'_{pq} of the rotated image is given by

$$A'_{pq} = A_{pq} e^{-jq\alpha}. \tag{6}$$

Thus, the magnitudes of the Zernike moments can be used as rotationally invariant image features.

The aforementioned favorable properties of the Zernike moments are valid as long as one uses a true analog image function. In practice, the Zernike moments have to be computed from sampled data. Thus, let us define the following discrete version of A_{pq} over the pixel set $\{(x_i, y_j), 1 \le i \le n, 1 \le j \le n\}$:

$$\hat{A}_{pq} = \sum_{x_i^2 + y_j^2 \le 1} \sum h_{pq}(x_i, y_j) f(x_i, y_j), \tag{7}$$

where

$$h_{pq}(x_i, y_j) = \int_{x_i - \frac{\Delta x}{2}}^{x_i + \frac{\Delta x}{2}} \int_{y_j - \frac{\Delta y}{2}}^{y_j + \frac{\Delta y}{2}} V_{pq}^*(x,y) dxdy \tag{8}$$

represents the integration of $V_{pq}^*(x, y)$ over the (i, j) pixel. Since the image function is defined over the unit disk, the summation in (7) takes into account only those pixels whose centers fall completely inside the circle. It is important to observe that even if $f(x, y) = 1$ for all $(x, y) \in D$, then

$$\hat{A}_{pq} \ne A_{pq}. \tag{9}$$

This is in sharp contrast with the digital approximation for the geometric and Legendre moments for which there is equality in (9), see [9].

Hence, there is an inherent error in computing $\hat{A}_{pq}$ which is related to the circular nature of the support of $\{V_{pq}(x, y)\}$. In what follows, we refer to such an error as the geometric error. For a general image function, not necessarily constant, the error between $\hat{A}_{pq}$ and A_{pq} can be decomposed as

$$E_{pq} = \hat{A}_{pq} - A_{pq} = E_{pq}^g + E_{pq}^n, \tag{10}$$

where E_{pq}^g is the geometric error and E_{pq}^n is the numerical error related to the need of numerical integration in (8). The geometric and numerical error components of the overall error (10) are studied in the following section.

3 Error Analysis

In this section, we examine two sources of error in $\hat{A}_{pq}$, i.e., the geometric and numerical errors.

3.1 Geometric Error

In order to reveal the fundamental nature of the geometric error, we consider the following expression

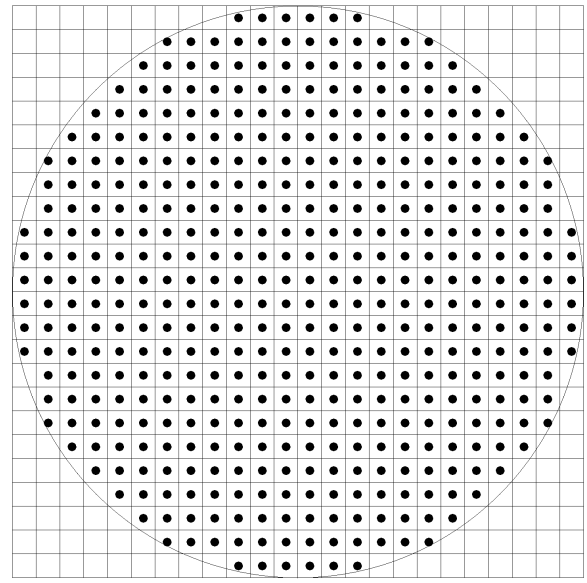

Fig. 1. Lattice-point approximation of a circular region.

$$G(n) = \frac{4}{n^2} \left[\sum_{(x_i, y_j) \in D} \sum 1 \right] - \pi. \tag{11}$$

This is equal to $\hat{A}_{00} - A_{00}$ provided that $f(x, y) = 1$ for all $(x, y) \in D$. In fact, let us observe that $\int\int_D V_{pq}^*(x,y) dxdy = \pi$, $V_{00}^*(x, y) = 1$, and that in our case, the unit disk is located in the $[-1, 1]^2$ square which is composed of n^2 pixels, i.e., $\Delta x = \Delta y = 2/n$.

The term $G(n)$ is not equal to zero due to the fact that if the center of a pixel falls inside the border of the unit disk $\{(x, y) : x^2 + y^2 \le 1\}$, this pixel is used in the computation of the Zernike moments; otherwise, the pixel is discarded. Therefore, the area used for the moment computing is not equal to that of the unit disk. Fig. 1 shows the union of the pixels whose centers fall inside the unit circle. Note that some pixels are not entirely inside the circle; on the other hand, some parts of the circle are not covered by pixels.

The quantity

$$K(n) = \sum_{(x_i, y_j) \in D} \sum 1$$

in (11) denotes the number of the points $\{(x_i, y_j) : 1 \le i, j \le n\}$ inside the unit circle. Hence, $G(n)$ can be rewritten as

$$G(n) = \frac{4}{n^2} K(n) - \pi. \tag{12}$$

The formula in (12) fully describes the nature of the geometric error, and it is crucial to know the size of $G(n)$, i.e., how fast $G(n)$ tends to zero as $n \to \infty$. This turns out not to be a trivial problem [6]. Nevertheless, the quantity $G(n)$ has been extensively examined in the analytic number theory with the relation to the so-called lattice points of a circle problem due originally to Gauss [5], [6]. Gauss' problem on the number of points inside a circle is to determine the correct order of magnitude of $G(n)$ as $n \to \infty$. First of all, it is known after Gauss that $G(n) = O(n^{-1})$. This result was improved by Sierpinski in 1906 to the form of $G(n) = O(n^{-4/3})$. Generally $G(n) = O(n^{-2(1-\theta)})$, $1/4 \le \theta \le 1/2$ with the following significant steps in the history of finding the smallest possible θ:

- Gauss (1834), $\theta = \frac{1}{2} = 0.5$;
- Sierpinski (1906), $\theta = \frac{1}{3} = 0.3333\ldots$;
- Walfisz (1927), $\theta = \frac{163}{494} = 0.329959514\ldots$;
- Titchmarsh (1935), $\theta = \frac{15}{46} = 0.326086957\ldots$;
- Hua (1942), $\theta = \frac{13}{40} = 0.325$;

and the most resent result by

- Iwaniec and Mozzochi [6] (1988), $\theta = \frac{7}{22} = 0.318181818\ldots$.

See also [5] for a slightly sharper result, equivalent to the latter one up to a logarithmic factor. Hardy's conjecture says that the value of θ can be arbitrary close to $\theta = 1/4 = 0.25$. It is also known that $\theta = 1/4$ is impossible. This still remains an open problem in analytic number theory. See [5], [6], and the references cited therein.

Hence, with the latest result due to Iwaniec and Mozzochi [6], we have the following result for the size of $G(n)$

$$G(n) = O(n^{-15/11}). \tag{13}$$

The relationship of $G(n)$ to the geometric error in the decomposition proposed in (10) is described by the following result.

THEOREM 1. *Let f be a bounded function on D. Then for any $p, q \geq 0$ we have*

$$\left|E_{pq}^{g}\right| \leq \bar{f}\left\{\frac{\pi}{p+1}\right\}^{\frac{1}{2}} G^{\frac{1}{2}}(n), \tag{14}$$

where $G(n)$ is defined in (12) *and* $\bar{f} = \max_{x,y} f(x,y)$.

The proof of Theorem 1 is deferred to the Appendix, where we also give the precise formula for E_{pq}^{g}. The decaying rate of E_{pq}^{g} is limited by the best possible result for the lattice approximation of the unit circle. By virtue of the Hardy's conjecture, the rate for E_{pq}^{g} can never exceed $O(n^{-3/4+\delta})$ for an arbitrary small $\delta > 0$. With the best possible result known so far due to Iwaniec and Mozzochi [6], the geometric error is of order $O(n^{-15/22})$.

3.2 Numerical Error

The numerical error is caused by the need of calculating two-dimensional integrals appearing in the definition of A_{pq}. The following result describes the size of the numerical error in the decomposition proposed in (10) for a wide class of image functions.

THEOREM 2. *Let f be a function of bounded variation on D. Then for any $p, q \geq 0$ we have*

$$\left|E_{pq}^{n}\right| \leq \left\{\frac{4\bar{f}\pi}{p+1} V(f)\right\}^{\frac{1}{2}} n^{-1}, \tag{15}$$

where $V(f)$ is the total variation of f, $\bar{f} = \max_{x,y} f(x,y)$.

The proof of Theorem 2 is deferred to the Appendix, where we also give the precise formula for E_{pq}^{n}. It is worth noting that the bound for the numerical error can be further improved if stronger than bounded variation assumption on the image function $f(x, y)$ is imposed, e.g., that $f(x, y)$ has a number of derivatives. Then the decreasing rate of E_{pq}^{g} can be faster than $O(n^{-1})$. Nevertheless from a practical point of view, we need to evaluate the factor $h_{pq}(x_i, y_j)$ defined in (8). For small values of q and p, this can be done by a direct integration in (8). For moderate and large values of p and q, some numerical integration techniques are needed.

The simplest strategy is the one-dimensional rule to approximate $h_{pq}(x_i, y_j)$ as

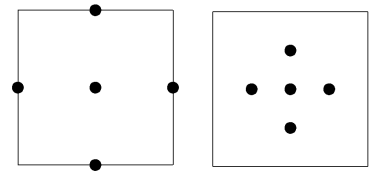

Fig. 2. Five-dimensional cubature formulas I and II.

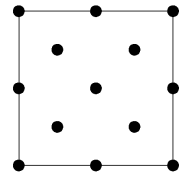

Fig. 3. The 13-dimensional cubature formula.

$$h_{pq}(x_i, y_j) \cong \Delta x \Delta y V_{pq}^{*}(x_i, y_j) \tag{16}$$

with the approximation error of order $O((\Delta x \Delta y)^2)$.

The L-order dimensional rules are of the general form

$$h_{pq}(x_i, y_j) \cong \Delta x \Delta y \sum_{l=1}^{L} w_l V_{pq}^{*}(u_l, v_l), \tag{17}$$

where $\{(u_l, v_l), 1 \leq l \leq L\}$ is a set of design points belonging to the (i, j) pixel centered at (x_i, y_j) and $\{w_l, 1 \leq l \leq L\}$ is a set of weights [3]. With an appropriate selection of the design points and weights, one can reduce the approximation error in (17) to $O((\Delta x \Delta y)^{L+1})$ and therefore to achieve a subpixel accuracy.

For simplicity of notation, let us denote $(\pm 1, \pm 1)$ the corner points of an individual pixel. Then the five-dimensional cubature formula (see Fig. 2a) for calculating $\int_{-1}^{1}\int_{-1}^{1} V(x,y)dxdy$, where $V(x, y)$ is some bivariate function, is given by

$$C_5^{I}(V) = \frac{1}{3}\{8V(0,0) + V(0,1) + V(1,0) + V(0,-1) + V(-1,0)\}. \tag{18}$$

Another type of the five-dimensional cubature formula shown in Fig. 2b is defined as

$$C_5^{II}(V) = \frac{4}{3}\{-V(0,0) + V(0,0.5) + V(0.5,0) + V(0,-0.5) + V(-0.5,0)\} \tag{19}$$

The number of nodes in each pixel can be increased further to achieve even higher accuracy. An example is to use the 13-dimensional cubature formula, whose nodes are shown in Fig. 3.

Two different ways of calculating weights yield the following formulas referred to as the 13-D(I) and 13-D(II) integration methods, respectively:

$$\begin{aligned} C_{13}^{I}(V) = \frac{1}{45}\{&120V(0,0) + 8[V(1,1) + V(1,-1) + V(-1,-1) + V(-1,1)] \\ &+16[V(0.5,0.5) + V(0.5,-0.5) + V(-0.5,-0.5) + V(-0.5,0.5)] \\ &-9[V(0,1) + V(1,0) + V(0,-1) + V(-1,0)]\} \end{aligned} \tag{20}$$

and

$$C_{13}^{II}(V) =$$
$$\frac{1}{45}\Big\{104V(0,0) + 4\Big[V(1,1) + V(1,-1) + V(-1,-1) + V(-1,1)\Big]$$
$$+16\Big[V(0.5,0.5) + V(0.5,-0.5) + V(-0.5,-0.5) + V(-0.5,0.5)\Big]$$
$$-\Big[V(0,1) + V(1,0) + V(0,-1) + V(-1,0)\Big]\Big\} \quad (21)$$

We refer to [8] for further details on the above two-dimensional numerical integration techniques.

Generally, the higher-dimensional integration rules are more accurate for calculating two-dimensional integrals. It should be stressed, however, that this is not the case in our situation since we are dealing with circular area. In fact, for multidimensional cubature formulas, some $V_{pq}^{*}(u_l, v_l)$ used in the computation of $h_{pq}(x_i, y_j)$ do not satisfy the restriction $u_l^2 + v_l^2 \le 1$. For example, there are 40, 16, and 140 design points falling outside the unit disk for formula C_5^I, C_5^{II}, and both C_{13}^I and C_{13}^{II}, respectively. Note that there is no such difficulty with the one-dimensional rule in (16). Nevertheless, a certain form of truncation applied to the multidimensional integration formulas can lead to their substantial improvement.

Let us redefine the Zernike moments in (7) as

$$\hat{A}_{pq}(\gamma) = \sum_{x_i^2 + y_j^2 \le 1-\gamma} \sum h_{pq}(x_i, y_j) f(x_i, y_j), \quad (22)$$

where γ is a small adjustable parameter. Observe that $\hat{A}_{pq}(0) = \hat{A}_{pq}$. The choice $\gamma = \frac{\sqrt{2}}{n}$ implies that only pixels completely falling into the unit circle are taken into account in (22). This, however, increases the geometric error, i.e., leads to poorer digital approximation of the circle. A less conservative choice is

$$\gamma = \frac{1}{n} + \varepsilon, \quad (23)$$

where ε is a small number, e.g., $\varepsilon = 0.0001$. With this choice, the number of the design points falling outside the unit disk will be reduced to 16, zero, 68 for the formula C_5^I, C_5^{II}, and both C_{13}^I and C_{13}^{II}, respectively. We will show the efficiency of the above modification of the Zernike moments in Section 5.

4 Image Reconstruction From $\{\hat{A}_{pq}\}$

In order to assess the performance of a set of image descriptors, one can look at their reconstruction power. Using (4) and replacing A_{pq} with $\hat{A}_{pq}$, we can define the following reconstruction algorithm

$$\hat{f}_T(x,y) = \sum_{p=0}^{T} \sum_{q=-p}^{p} \tau_p \hat{A}_{pq} V_{pq}(x,y), \quad p - |q| = \text{even}, \quad (24)$$

where T is the truncation parameter informing us how many moments are taken into account.

The energy of the error $\hat{f}_T(x,y) - f(x,y)$ can serve as a natural performance measure for $\hat{f}_T(x,y)$, i.e.,

$$Error(\hat{f}_T) = \iint_D \left|\hat{f}_T(x,y) - f(x,y)\right|^2 dxdy. \quad (25)$$

By virtue of (3) and Parseval's formula, we obtain the following decomposition for $Error(\hat{f}_T)$:

$$Error(\hat{f}_T) = \sum_{p=0}^{T} \sum_{q=-p}^{p} \tau_p \left|\hat{A}_{pq} - A_{pq}\right|^2 + \sum_{p=T+1}^{\infty} \sum_{q=-p}^{p} \tau_p \left|A_{pq}\right|^2 = D_T + F_T, \quad (26)$$

where $p - |q|$ = even. Note that the term F_T is a result of using a finite number of moments in the reconstruction algorithm. It is also clear that D_T increases with T, whereas F_T decreases with T. This reveals that there is T^* which minimizes an apparent trade-off between the terms in (26). In order to find such an optimal T, let us evaluate D_T and F_T.

Concerning the term D_T in (26), it is sufficient to evaluate the difference $\left|\hat{A}_{pq} - A_{pq}\right|$ which (as it has been suggested in (10)) can be decomposed into two components describing the discretization and geometric errors.

The results of Theorems 1 and 2 readily lead to the following bound for $\left|\hat{A}_{pq} - A_{pq}\right|$.

THEOREM 3. *Under the assumptions of Theorem 2, we have*

$$\left|\hat{A}_{pq} - A_{pq}\right| \le \left\{\frac{4\bar{f}\pi}{p+1} V(f)\right\}^{1/2} n^{-1} + \bar{f}\left\{\frac{\pi}{p+1}\right\}^{1/2} G^{1/2}(n). \quad (27)$$

With the help of the best known result from the number theory, see (13), we can conclude that the geometric error dominates the magnitude of $\left|\hat{A}_{pq} - A_{pq}\right|$, i.e., we have

$$\left|\hat{A}_{pq} - A_{pq}\right| = O\left(n^{-15/22}\right). \quad (28)$$

Furthermore, the application of Theorem 3 in (26) yields the following bound for the term D_T in the decomposition of the $Error(\hat{f}_T)$:

$$D_T \le 2\bar{f}\left(4V(f)n^{-2} + \bar{f}G(n)\right)\sum_{p=0}^{T}(p+1)$$
$$= \bar{f}\left(4V(f)n^{-2} + \bar{f}G(n)\right)(T+1)(T+2) \quad (29)$$

By this and (13), it follows that D_T is of order

$$D_T = O\left(\frac{T^2}{n^{\frac{15}{11}}}\right). \quad (30)$$

Concerning the term F_T in (26), let us observe that $F_T \to 0$ as $T \to \infty$. The rate at which $F_T \to 0$ depends on the smoothness of the image function $f(x, y)$, i.e., the smoother $f(x, y)$ is the faster F_T tends to zero.

For the class of bounded variation functions, by using the Picone's and Jackson's theorem [13, p. 202], one can prove that

$$\left|A_{pq}\right| = O\left(\frac{1}{(p+1)(p+2)^{1/2}(q+1)}\right). \quad (31)$$

Consequently

$$F_T = \sum_{p=T+1}^{\infty} \sum_{q=-p}^{p} \tau_p \left|A_{pq}\right|^2 \le c_1 \sum_{p=T+1}^{\infty} \sum_{q=-p}^{p} \frac{1}{(p+1)(p+2)(q+1)^2}$$
$$\le c_2 \sum_{p=T+1}^{\infty} \frac{1}{(p+1)(p+2)} = O\left(\frac{1}{T}\right) \quad (32)$$

where c_1 and c_2 are some positive constants.

Combining (30) and (32), we can obtain the following bound for $Error(\hat{f}_T)$ valid for all image functions of the bounded variation class:

$$Error(\hat{f}_T) = O\left(\frac{T^2}{n^{15/11}}\right) + O\left(\frac{1}{T}\right). \quad (33)$$

Thus, the truncation parameter T minimizing this bound is of the form

$$T^* = cn^{5/11}, \quad (34)$$

Fig. 4. Five original Chinese characters used in image reconstruction via Zernike moments. From left to right are C_1, C_2, C_3, C_4, and C_5.

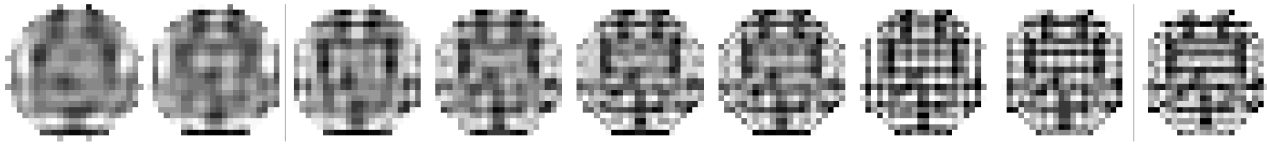

Fig. 5. Reconstructed patterns of the character C_1 based on the Zernike moments of order 14, 16, 18, 20, 22, 24, 26, 28, and 30.

for some constant $c > 0$. The optimal choice of T says how many moments should be taken into account in order to achieve the smallest possible reconstruction error. This gives the accuracy of our reconstruction method of the order

$$Error\left(\hat{f}_{T^*}\right) = O\left(n^{-5/11}\right). \tag{35}$$

One can conjecture that this is an optimal rate of convergence for $\hat{f}_T$ within the class of image functions of bounded variation. Exact constants in the above bounds can be computed for particular image functions.

5 Experimental Results

A set of five Chinese characters is employed as the test images. Each image consists of 24×24 pixels and the range of gray levels for each pixel is 32, where all characters have the gray level 11 and the background has the value 21. Fig. 4 illustrates these five Chinese characters projected onto the unit disk.

5.1 Traditional Zernike Moment Method

Here we calculate A_{pq} employing the simplest one-dimensional integration formula in (16). The normalized mean square error

$$\overline{Error}\left(\hat{f}_T\right) = \frac{\iint_D \left|f(x,y) - \hat{f}(x,y)\right|^2 dxdy}{\iint_D \left[f(x,y)\right]^2 dxdy} \tag{36}$$

is adopted as a measure of the accuracy of the reconstructed images.

The Chinese character C_1 is used as the test image. Fig. 5 illustrates the reconstructed images of C_1. The first pattern is reconstructed from moments of order 14, then from left to right, are the reconstructed images from moments of order 16, 18, 20, 22, 24, 26, 28, and 30, respectively.

5.2 Modified Zernike Moment Method

We have introduced a modified version $\hat{A}_{pq}(\gamma)$ of the Zernike moments in (22) of Section 3.2. In our experiment, the parameter γ is chosen as $\gamma = n^{-1} + 0.0001$.

For the sake of comparison, the same Chinese character C_1 is employed as the test image, and the normalized mean square error defined in (36) is used.

Fig. 6 shows the $\overline{Error}\left(\hat{f}_T\right)$ values for all five types of numerical integration formulas as a function of the moment order. Fig. 6 indicates that all of four new proposed integration formulas perform better than the simple one-dimensional integration formula of the traditional Zernike moment method. Among the applied integration techniques, the five-dimensional formula C_5^{II} is superior to the other techniques and therefore seems to be the best candidate for the image reconstruction for this specific situation. The reason that C_5^{II} provides better result is that with the new condition for the Zernike moments, all nodes used in this formula fall inside the unit disk. For C_5^I and both C_{13}^I and C_{13}^{II}, there are 16 and 68 nodes falling outside the unit disk, respectively.

The reconstructed images of the character C_1 with five integration formulas are shown in Fig. 7. The first row shows the reconstructed patterns from the one-dimensional integration formula, whereas the second, third, fourth, and fifth rows show C_5^I, C_5^{II}, C_{13}^I, and C_{13}^{II}, correspondingly. All images in the first column are reconstructed from moment of order 10, then from left to right, of order 15, 20, 25, 30, 35, and 40, respectively.

By using the integration formula C_5^{II}, we reconstructed all five Chinese characters shown in Fig. 4 with the Zernike moments of orders from 20 to 48. Fig. 8 depicts the reconstructed images.

6 Conclusions

In this paper, we have studied the accuracy problem for Zernike moments determined from discrete data observed on the $n \times n$ pixels image domain. It has been observed that two kinds of errors determine the accuracy of Zernike moments computing, i.e., the numerical error related to the usual need of calculating two-dimensional integrals and the geometric error being a distinctive feature of Zernike moments. We have shown that the geometric error plays a critical role for the accuracy of the Zernike moments computing. Employing the most recent results from number theory on the lattice points of a circle, we establish that the error of estimation of the Zernike moments is of order $O\left(n^{-\frac{15}{22}}\right)$.

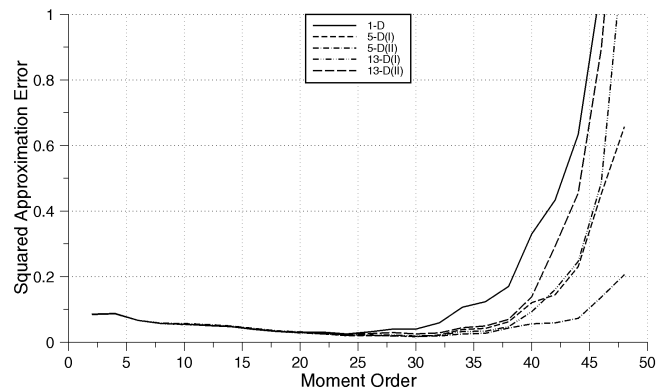

Fig. 6. The normalized reconstruction error for the reconstructed character C_1 via the proposed Zernike moment technique with five numerical integration formulas.

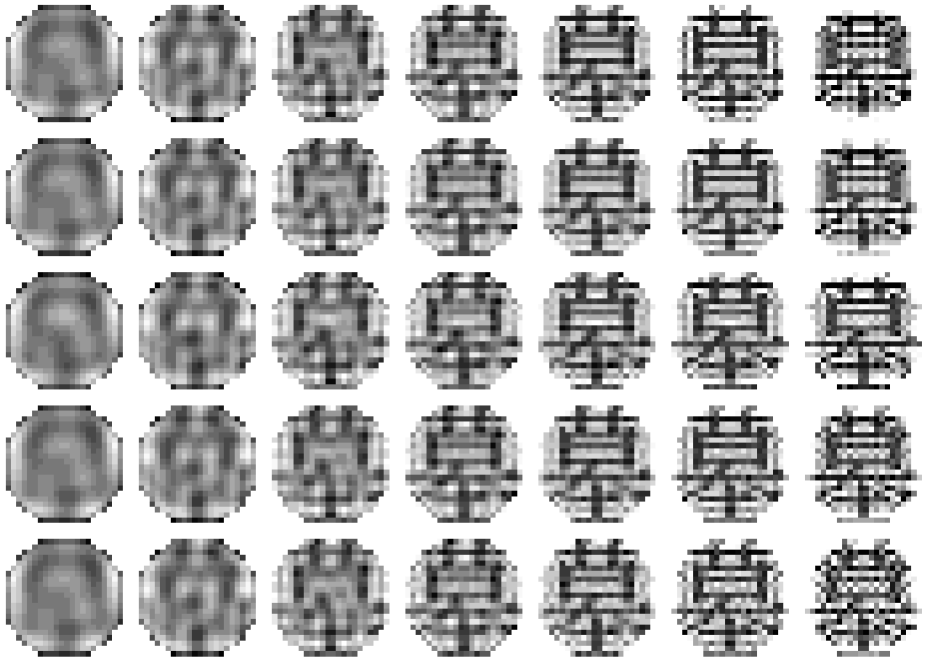

Fig. 7. Reconstructed patterns of the character C_1 using the modified method and five different integration rules. From left to right, the results based on moments of order 10, 15, 20, 25, 30, 35, and 40.

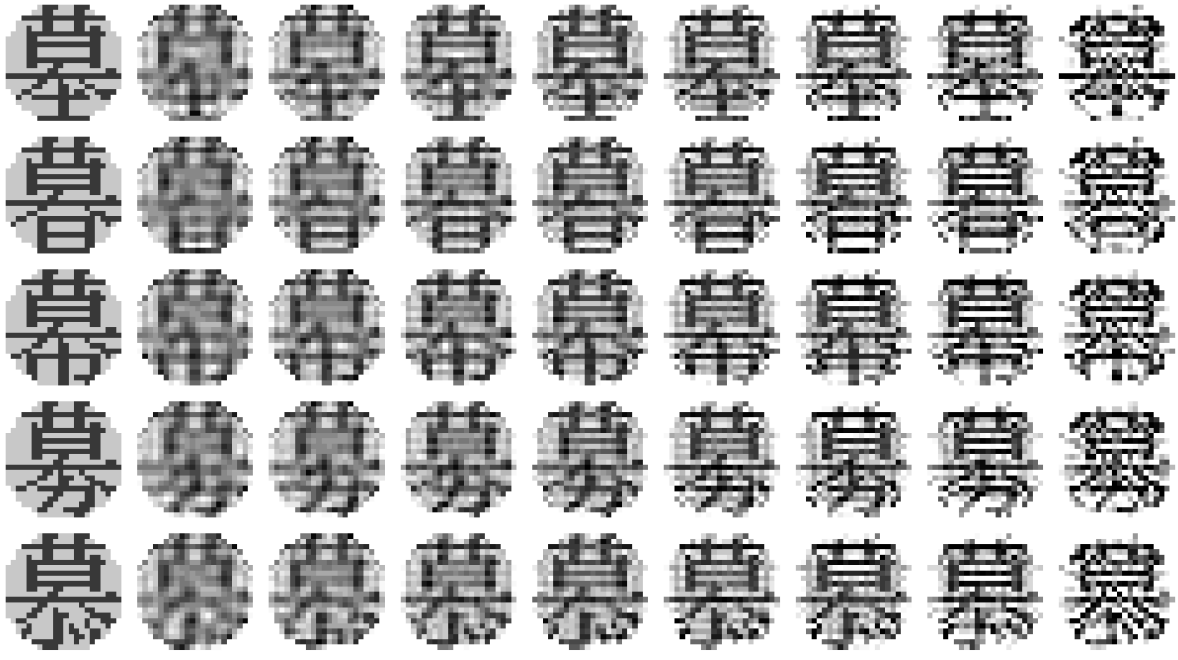

Fig. 8. Reconstructed patterns of the five Chinese characters based on the integration formula C_5^{II}. From the left to right are the original characters, the reconstructed characters utilizing the modified Zernike moments of order 20, 24, 28, 32, 36, 40, 44, and 48.

The numerical error related to the computation of the Zernike moments is studied as well. We have introduced some multidimensional cubature formulas and a modified version of the Zernike moments in order to decrease the computation errors. With the increased overall accuracy in the Zernike moments computing, we have reconstructed some images from finite Zernike moments. We also evaluated the integrated squared error of the reconstruction technique based on the maximum T order estimated Zernike moments. For a large class of image functions, we have found that the optimal value of T minimizing the reconstruction error is of order $n^{5/11}$. The corresponding minimal value of the reconstruction error is $O\left(n^{-\frac{5}{11}}\right)$.

APPENDIX
PROOF OF THEOREM 1 AND THEOREM 2

Let $D = \{(x, y) : x^2 + y^2 \le 1\}$ be the unit disk. Let p_{ij} denote the (i, j) pixel at (x_i, y_j). Note that the area of a single pixel is $4/n^2$, where n^2 is the total number of pixels.

Redefining the (p, q) Zernike polynomial as $V_{pq}(x, y)$ on D and zero otherwise, we can decompose A_{pq} as

$$A_{pq} = \sum_{(x_i,y_j)\in D} \sum \int\int_{p_{ij}} f(x,y)V_{pq}^*(x,y)dxdy + \int\int_{O(n)} f(x,y)V_{pq}^*(x,y)dxdy, \quad (37)$$

where $O(n)$ is the region being the intersection of D with the union of those pixels whose centers and corners fall outside the circle.

Using (37), we can write the following decomposition for $\hat{A}_{pq} - A_{pq}$:

$$\hat{A}_{pq} - A_{pq} = \sum_{(x_i,y_j)\in D} \sum \int\int_{p_{ij}} \left(f(x_i,y_j) - f(x,y)\right)V_{pq}^*(x,y)dxdy - \int\int_{O(n)} f(x,y)V_{pq}^*(x,y)dxdy \quad (38)$$

The first term of this decomposition defines the numerical error E_{pq}^n, while the second the geometric error E_{pq}^g, i.e.,

$$E_{pq}^n = \sum_{(x_i,y_j)\in D} \sum \int\int_{p_{ij}} \left(f(x_i,y_j) - f(x,y)\right)V_{pq}^*(x,y)dxdy, \quad (39)$$

$$E_{pq}^g = -\int\int_{O(n)} f(x,y)V_{pq}^*(x,y)dxdy. \quad (40)$$

Let us first consider the term E_{pq}^n. By virtue of Cauchy-Schwartz inequality for integrals and sums, we have

$$\left|E_{pq}^n\right| \le \sum_{(x_i,y_j)\in D} \sum \left\{\int\int_{p_{ij}\cap D} \left(f(x_i,y_j) - f(x,y)\right)^2 dxdy \int\int_{p_{ij}} \left|V_{pq}^*(x,y)\right|^2 dxdy\right\}^{\frac{1}{2}}$$

$$\le \left\{\sum_{(x_i,y_j)\in D} \sum \int\int_{p_{ij}\cap D} \left(f(x_i,y_j) - f(x,y)\right)^2 dxdy \int\int_{D} \left|V_{pq}^*(x,y)\right|^2 dxdy\right\}^{\frac{1}{2}}$$

Arguing as in the proof of Theorem 1 in [9], we can show that for f being a bounded variation function, we have

$$\sum_{(x_i,y_j)\in D} \sum \int\int_{p_{ij}\cap D} \left(f(x_i,y_j) - f(x,y)\right)^2 dxdy \le 4\frac{\bar{f}}{n^2} V(f),$$

where $V(f)$ is the total variation of f and $\bar{f} = \max_{x,y} f(x,y)$.

Furthermore, due to (3), we have

$$\int\int_D \left|V_{pq}^*(x,y)\right|^2 dxdy = \frac{\pi}{p+1}.$$

All these considerations lead to

$$\left|E_{pq}^n\right| \le \left\{\frac{4\pi\bar{f}}{p+1} V(f) n^{-2}\right\}^{\frac{1}{2}}. \quad (41)$$

This proves Theorem 2. □

Let us now take the geometric error E_{pq}^g into account. By Cauchy-Schwartz inequality, we have

$$\left|E_{pq}^g\right| \le \left\{\int\int_{O(n)} f^2(x,y)dxdy \int\int_D \left|V_{pq}^*\right|^2 dxdy\right\}^{\frac{1}{2}} \le \bar{f}\left\{\frac{\pi}{p+1}\left|O(n)\right|\right\}^{\frac{1}{2}}, \quad (42)$$

where $|O(n)|$ is the area of the set $O(n)$. The discussion in Section 3.1 yields an important observation that

$$|O(n)| \le |G(n)|,$$

where $G(n)$ is the remainder term of the lattice approximation of D, see (12).

This proves Theorem 1. □

ACKNOWLEDGMENTS

We extend our thanks to the referees for the detailed and constructive comments. The authors are supported by grants from NSERC.

REFERENCES

[1] R.R. Bailey and M. Srinath, "Orthogonal Moment Feature for Use With Parametric and Non-Parametric Classifiers," *IEEE Trans. Pattern Analysis and Machine Intelligence*, vol. 18, pp. 389-396, 1996.

[2] A.B. Bhatia and M. Born, "On the Circle Polynomials of Zernike and Related Orthogonal Sets," *Proc. Cambridge Philosophical Soc.*, vol. 50, pp. 40-53, 1954.

[3] H. Engels, *Numerical Quadrature and Cubature*. London: Academic Press Inc., 1980.

[4] M.K. Hu, "Visual Problem Recognition by Moment Invariant," *IRE Trans. Information Theory*, vol. 8, pp. 179-187, Feb. 1962.

[5] M.N. Huxley, "Exponential Sums and Lattice Points," *Proc. London Math. Soc.*, vol. 60, pp. 471-502, 1990.

[6] H. Iwaniec and C.J. Mozzochi, "On the Divisor and Circle Problems," *J. Number Theory*, vol. 29, pp. 60-93, 1988.

[7] A. Khotanzad and Y.H. Hong, "Invariant Image Recognition by Zernike Moments," *IEEE Trans. Pattern Analysis and Machine Intelligence*, vol. 12, pp. 489-498, 1990.

[8] S. X. Liao, "Image Analysis by Moments," PhD dissertation, Univ. of Manitoba, 1993.

[9] S.X. Liao and M. Pawlak, "On Image Analysis by Moments," *IEEE Trans. Pattern Analysis and Machine Intelligence*, vol. 18, pp. 254-266, 1996.

[10] R. Mukundan and K.R. Ramakrishnan, "Fast Computation of Legendre and Zernike Moments," *Pattern Recognition*, vol. 28, pp. 1,433-1,442, 1995.

[11] M. Pawlak, "On the Reconstruction Aspects of Moment Descriptors," *IEEE Trans. Information Theory*, vol. 38, no. 6, pp. 1,698-1,708, Nov. 1992.

[12] R.J. Prokop and A.P. Reeves, "A Survey of Moment-Based Techniques for Unoccluded Object Representation and Recognition," *Graphical Models and Image Processing*, vol. 54, no. 5, pp. 438-460, Sept. 1992.

[13] G. Sansone, *Orthogonal Functions*. New York: Dover Publications, Inc., 1991.

[14] M.R. Teague, "Image Analysis via the General Theory of Moments," *J. Optical Soc. Am.*, vol. 70, pp. 920-930, Aug. 1980.

[15] C.H. Teh and R.T. Chin, "On Digital Approximation of Moment Invariants," *Computer Vision, Graphics, and Image Processing*, vol. 33, pp. 318-326, 1986.

[16] C.H. Teh and R.T. Chin, "On Image Analysis by the Methods of Moments," *IEEE Trans. Pattern Analysis and Machine Intelligence*, vol. 10, pp. 496-512, July 1988.

[17] O.D. Trier, A.K. Jain, and T. Taxt, "Feature Extraction Methods for Character Recognition—A Survey," *Pattern Recognition*, vol. 29, pp. 641-701, 1996.

[18] F. Zernike, "Beugungstheorie des Schneidenverfahrens und seiner verbesserten Form, der Phasenkontrastmethode," *Physica*, vol. 1, pp. 689-701, 1934.